Archives of Hydro-Engineering and Environmental Mechanics
Vol. 51 (2004), No. 2, pp. 149–181

Effect of Heterogeneity on Shear Zone Formation during Plane Strain Compression

Jacek Tejchman

Civil Engineering Department, Gdańsk University of Technology
80-952 Gdańsk, Narutowicza 11/12, Poland, e-mail: tejchmk@pg.gda.pl

(Received December 02, 2003; revised April 28, 2004)

Abstract

Heterogeneity of granular materials triggers shear zone formation. In the paper, the FE-analysis of the effect of the material heterogeneity on the formation of a spontaneous shear zone inside of granular materials during a plane strain compression test is presented. The numerical calculations are performed with a finite element method on the basis of a hypoplastic constitutive law extended by polar quantities: rotations, curvatures and couple stresses. A mean grain diameter is used as a characteristic length. The constitutive law takes into account the effect of pressure, void ratio, direction of deformation rate and mean grain diameter on the behaviour of granular bodies. The heterogeneity in the granular body is assumed in the form of spots with a different initial void ratio. The spots are single or distributed randomly and stochastically with an exponential probability function. The single spots are distributed sparsely and densely in an initially dense and loose granular specimen. Special attention is focused on the effect of heterogeneity on the onset of shear localization and its thickness at residual state.

Key words: heterogeneity, mean grain diameter, polar continuum, shear zone, void ratio

1. Introduction

Localization of deformation in narrow shear zones is a fundamental phenomenon of granular material behaviour (Vardoulakis 1977, 1980, Tejchman 1989, 1997, Yoshida et al 1994, Tatsuoka et al 1994, 1997, Desrues et al 1996, Leśniewska 2000, Nübel 2002). Shear localizations are accompanied by pronounced grain rotations (Oda et al 1982, Uesugi et al 1988, Löffelmann 1989) and curvatures connected to couple stresses (Oda 1993), large strain gradients (Vardoulakis 1980) and void ratio changes (Desrues et al 1996, Oda et al 1997). Since shear localization is a precursor of failure of soils, shear localization has to be taken into account when modelling granular materials. Therefore, the constitutive law has to include a characteristic length to describe the thickness of shear zones and

spacing between them. There are several approaches to capture spontaneous and induced shear localizations in granular bodies in a quasi-static regime: strain gradient (Aifantis 1984, Sluys 1992, de Borst et al 1992, Pamin 1994, Zervos et al 2001, Maier 2002, Tejchman 2004b), non-local (Bazant and Lin 1988, Brinkgreve 1994, Marcher and Vermeer 2001, Maier 2002, Tejchman 2003b, 2004a) and polar ones (Mühlhaus 1989, 1990, Tejchman 1989, 1997, de Borst 1991, Tejchman and Wu 1993, Steinmann 1995). These approaches regularize the ill-posedness caused by the localization formation (differential equations of motion do not change their elliptic type during quasi-static calculations). Thus, the mesh-independent results are provided. Otherwise, FE-results are completely controlled by the size and orientation of the mesh and thus produce unreliable results, i.e. the shear zones become narrower upon mesh refinement (element size becomes the characteristic length) and computed force-displacement curves change considerably depending on the thickness of the calculated shear zone (Tejchman 1997).

The experimental results show that the thickness of shear zones depends on many different factors such as: pressure level, void ratio, direction of deformation, specimen size, mean grain diameter, grain roughness, grain hardness, surface roughness and stiffness of the surrounding structure in contact with a granular body. In addition, the distribution of microscopic inhomogeneities inherently present in granular materials and triggering shear localization seems to be an influential factor (Hobbs and Ord 1989, Tejchman and Wu 1993, 1995, Belytschko et al 1994, Gutierrez and de Borst 1998, Chambon et al 1998, Nübel and Karcher 1998, Tejchman 2002, Gudehus and Nübel 2003, Tejchman 2003a, Shi and Chang 2003). Thus, it is of major importance by modelling shear localizations to use a constitutive model taking all influential factors into account.

The intention of the paper was to show the effect of the distribution of heterogeneity on the formation of shear localization during a plane strain compression test with dry cohesionless sand specimen. The heterogeneity was assumed in the form of single spots with a different initial void ratio. The spots were fixed in an initially dense and loose granular specimen. The calculations were carried with weak and strong spots. The number of fixed spots varied from one to three. They were distributed sparsely with large spacing or densely with small spacing. In addition, the calculations were carried out with the initial void ratio distributed randomly and stochastically with an exponential frequency function. In a numerical analysis, a finite element method and a polar hypoplastic constitutive law were used. The law takes into account the effect of initial density, pressure, direction of deformation rate, mean grain size and grain roughness on shear localization. Due to the presence of a characteristic length in the form of mean grain diameter, the law can realistically describe the formation of shear zones. In the FE-analyses, the emphasis was placed on the influence of heterogeneity on the location and thickness of shear zones inside a granular specimen. Only the plane strain case

was taken into account. Other effects influencing the shear zone formation (loading eccentricity, non-uniform friction conditions along the specimen boundaries, sample preparation and sample dimensions) were not taken into account. A comprehensive analysis of the effect of different distributions of the initial void ratio on shear zone formation during compression has not been performed yet.

2. Hypoplasticity

Hypoplastic constitutive laws (Kolymbas 1977, Wu 1992, Bauer 1996, Gudehus 1996, von Wolffersdorf 1996) are an alternative to elasto-plastic formulations for continuum modelling of granular materials. They describe the evolution of effective stress components with the evolution of strain components by a differential equation including isotropic linear and non-linear tensorial functions according to the representation theorem by Wang (1970). They were formulated by a heuristic process (starting from hypoelastic models) considering all requirements which seem to be important for granular material behaviour. In contrast to elasto-plastic models, the decomposition of deformation components into elastic and plastic parts, yield surface, plastic potential, flow rule and hardening rule are not needed. The hypoplastic models describe the behaviour of so-called simple grain skeletons which are characterised by the following properties (Gudehus 1996):

- the state is fully defined through the skeleton pressure and void ratio (inherent anisotropy of contact forces between grains is not considered and vanishing principal stresses are not allowed),
- deformation of the skeleton is due to grain rearrangements (e.g. small deformations $< 10^{-5}$ due to elastic behaviour of grain contacts are negligible),
- grains are permanent (abrasion and crushing are excluded in order to keep the granulometric properties unchanged),
- three various void ratios decreasing exponentially with pressure are distinguished (minimum, maximum and critical),
- the material manifests an asymptotic behaviour for monotonous and cyclic shearing and proportional compression,
- rate effects are negligible,
- physico-chemical effects (capillary and osmotic pressure) and cementation of grain contacts are not taken into account.

The hypoplastic constitutive laws are of the rate type. Due to the incremental non-linearity with the deformation rate, they are able to describe both non-linear stress-strain and volumetric behaviour of granular bodies during shearing up to and after the peak with a single tensorial equation. They include also: barotropy (dependence on pressure level), pycnotropy (dependence on density), dependence on the direction of deformation rate, dilatancy and contractancy during shearing

with constant pressure, increase and release of pressure during shearing with constant volume, and material softening during shearing of a dense material. They are apt to describe stationary states, i.e. states in which a grain aggregate can continuously be deformed at constant stress and constant volume under a certain rate of deformation. Although, the hypoplastic models are developed without recourse to concepts of the theory of plasticity, failure surface, flow rule and plastic potential are obtained as natural outcomes (Wu and Niemunis 1996). The feature of the model is a simple formulation and procedure for determination of material parameters with standard laboratory experiments. The parameters are related to granulometric properties encompassing grain size distribution curve, shape, angularity and hardness of grains (Herle and Gudehus 1999). Owing to that, one set of material parameters is valid within a large range of pressures and densities.

Stress changes due to the deformation of a granular body can be generally expressed by

$$\overset{0}{\sigma}_{ij} = F(e, \sigma_{kl}, d_{kl}), \tag{1}$$

wherein the Jaumann stress rate tensor (objective stress rate tensor) is defined by

$$\overset{0}{\sigma}_{ij} = \overset{\bullet}{\sigma}_{ij} - w_{ik}\sigma_{kj} + \sigma_{ik}w_{kj}. \tag{2}$$

The function F in Eq. 1 represents an isotropic tensor-valued function of its arguments, σ_{ij} is the Cauchy skeleton (effective) stress tensor, e the void ratio and d_{kl} the rate of deformations tensor (stretching tensor). If the volume of grains remains constant (i.e. incompressible grains), the rate of the void ratio can be expressed by the evolution equation

$$\overset{*}{e} = (1+e)d_{kk}. \tag{3}$$

The rate of deformation tensor d_{ij} and the spin tensor w_{ij} are related to the material velocity v as follows:

$$d_{ij} = (v_{i,j} + v_{j,i})/2, \quad w_{ij} = (v_{i,j} - v_{j,i})/2, \quad ()_{,i} = \partial()/\partial x_i. \tag{4}$$

According to the condition of the incremental non-linearity (Wu 1992), the function F in Eq. 1 can be decomposed into two parts (it is not differentiable only at $d_{ij} = 0$):

$$\overset{0}{\sigma}_{ij} = A(e, \sigma_{kl}, d_{kl}) + B(e, \sigma_{ij})||d_{kl}||. \tag{5}$$

The function A is linear in d_{kl}, while the function B is non-linear in d_{kl} ($||d_{kl}||$ denotes the Euclidian norm $\sqrt{d_{kl}d_{kl}}$). Both functions are positively homogeneous of the first degree in d_{kl}, i.e. $\overset{0}{\sigma}_{kl}(\lambda d_{kl}) = \lambda \overset{0}{\sigma}_{kl} d_{kl}$ for any scalar $\lambda > 0$. In this way,

Eq. 5 becomes rate-independent. Due to that $\overset{0}{\sigma}_{kl}(+d_{kl}) \neq \overset{0}{\sigma}_{kl}(-d_{kl})$, the hypoplastic constitutive equation is incrementally non-linear, which allows for description of the inelastic behaviour. As a limit case during monotonous shearing, the critical state concept is also taken into account for both simultaneously vanishing both stress rates and volumetric deformation rate, and a constant void ratio ($\overset{0}{\sigma}_{ij} = 0$, $d_{kk} = 0$, $\dot{e} = 0$).

The following representation of the general constitutive equation (Eq. 6) is used (Bauer 1996, Gudehus 1996):

$$\overset{0}{\sigma}_{ij} = f_s \left[L_{ij} \left(\hat{\sigma}_{kl}, d_{kl} \right) + f_d N_{ij} \left(\hat{\sigma}_{ij} \right) \sqrt{d_{kl} d_{kl}} \right], \tag{6}$$

wherein the normalized stress tensor $\hat{\sigma}_{ij}$ is defined by

$$\hat{\sigma}_{ij} = \frac{\sigma_{ij}}{\sigma_{kk}}. \tag{7}$$

The scalar factors $f_s = f_s(e, \sigma_{kk})$ and $f_d = f_d(e, \sigma_{kk})$ take into account the influence of the density and pressure level on the stress. The stiffness factor f_s is proportional to the granulate hardness h_s and depends on the mean stress and void ratio:

$$f_s = \frac{h_s}{n h_i} \left(\frac{1 + e_i}{e} \right) \left(-\frac{\sigma_{kk}}{h_s} \right)^{1-n} \tag{8}$$

with

$$h_i = \frac{1}{c_1^2} + \frac{1}{3} - \left(\frac{e_{i0} - e_{d0}}{e_{c0} - e_{d0}} \right)^{\alpha} \frac{1}{c_1 \sqrt{3}}. \tag{9}$$

The granulate hardness h_s represents a density-independent reference pressure and it is related to the entire skeleton (not to single grains). The density factor f_d resembles a pressure-dependent relative density index and is represented by

$$f_d = \left(\frac{e - e_d}{e_c - e_d} \right)^{\alpha}. \tag{10}$$

Here e is the current void ratio, e_c is the critical void ratio, e_d denotes the void ratio at maximum densification (due to cyclic shearing), e_i is the maximum void ratio, and α denotes the pycnotropy coefficient, and n is the compression coefficient. The void ratio e is limited thus by e_i and e_d. The values of e_i, e_d and e_c are assumed to decrease with the pressure $-\sigma_{kk}$ according to the equations (Bauer 1996), Fig. 1:

$$e_i = e_{i0} \exp\left[-(-\sigma_{kk}/h_s)^n \right], \tag{11}$$

$$e_d = e_{d0} \exp\left[-(-\sigma_{kk}/h_s)^n \right], \tag{12}$$

$$e_c = e_{c0} \exp\left[-(-\sigma_{kk}/h_s)^n \right], \tag{13}$$

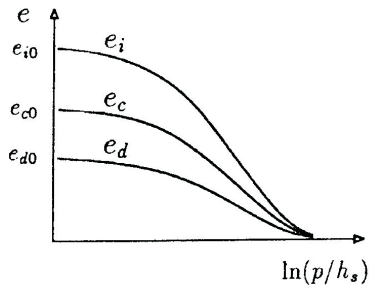

Fig. 1. Pressure dependence of void ratios

wherein e_{i0}, e_{d0} and e_{c0} are the values of e_i, e_d and e_c for $\sigma_{kk} = 0$, respectively. For the tensorial functions L_{ij} and N_{ij}, the following representatives are used (Bauer 1996, Gudehus 1996):

$$L_{ij} = a_1^2 d_{ij} + \hat{\sigma}_{ij} \hat{\sigma}_{kl} d_{kl}, \qquad N_{ij} = a_1 \left(\hat{\sigma}_{ij} + \hat{\sigma}_{ij}^* \right), \tag{14}$$

where

$$a_1^{-1} = c_1 + c_2 \sqrt{\hat{\sigma}_{kl}^* \hat{\sigma}_{lk}^*} \left[1 + \cos(3\theta) \right], \tag{15}$$

$$\cos(3\theta) = -\frac{\sqrt{6}}{\left[\hat{\sigma}_{kl}^* \hat{\sigma}_{kl}^* \right]^{1.5}} \left(\hat{\sigma}_{kl}^* \hat{\sigma}_{lm}^* \hat{\sigma}_{mk}^* \right), \tag{16}$$

$$c_1 = \sqrt{\frac{3}{8}} \frac{(3 - \sin\phi_c)}{\sin\phi_c}, \quad c_2 = \frac{3}{8} \frac{(3 + \sin\phi_c)}{\sin\phi_c}. \tag{17}$$

The parameter ϕ_c is the critical angle of internal friction during stationary flow and the parameter θ denotes the Lode angle; the angle on the deviatoric plane $\sigma_1 + \sigma_2 + \sigma_3 = 0$ between the stress vector and the axis σ_3(σ_i is the principle stress vector), and σ_{ij}^* denotes the deviatoric part of σ_{ij}. In case of sand, the hypoplastic constitutive relation is approximately valid in a pressure range 1 kPa $< -\sigma_{kk}/3 <$ 1000 kPa. Below it, additional capillary forces due to the air humidity and van der Waals forces may become important, and above it, grain crushing.

The constitutive relationship requires the following material constants: e_{i0}, e_{d0}, e_{c0}, ϕ_c, h_s, n and α. The FE-analyses were carried out with the material constants for so-called Karlsruhe sand: $e_{i0} = 1.30$, $e_{d0} = 0.51$, $e_{c0} = 0.82$, $\phi_c = 30^\circ$, $h_s = 190$ MPa, $n = 0.50$ and $\alpha = 0.30$ (Bauer 1996). The parameters h_s and n are estimated from a single oedometric compression test with an initially loose specimen (h_s reflects the slope of the curve in a semi-logarithmic representation, and n its curvature, Fig. 2). The constant α is found from a triaxial test with a dense specimen (it reflects the height and position of the peak value of the stress-strain

curve). The angle ϕ_c is determined from the angle of repose or measured in a triaxial test with a loose specimen. The values of e_{i0}, e_{d0}, e_{c0} are obtained with conventional index tests ($e_{c0} \approx e_{\max}$, $e_{d0} \approx e_{\min}$, $e_{i0} \approx (1.1 - 1.5)e_{\max}$). The mean grain diameter of sand is $d_{50} = 0.5$ mm.

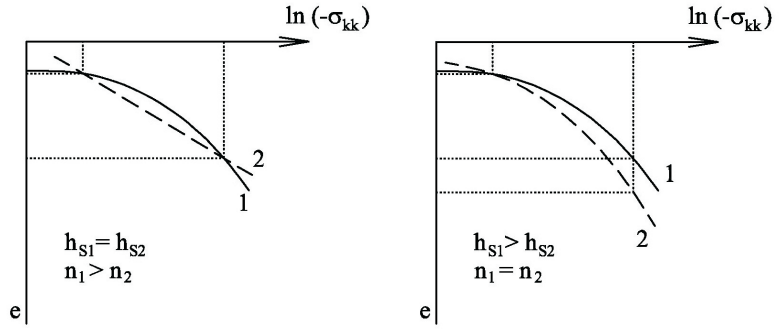

Fig. 2. Influence of n and h_s on compression curves for two different materials

A hypoplastic constitutive law cannot describe realistically shear localisation since it does not include a characteristic length. A characteristic length was taken into account by means of a polar theory (Schäfer 1962).

3. Polar Hypoplasticity

The polar terms were introduced in a hypoplastic law with the aid of a polar (Cosserat) continuum (Schäfer 1962, Mühlhaus 1989). A Cosserat continuum takes into account two linked levels of deformation: micro-deformation at the particle level and macro-deformation at the structural level. Each material point has for the case of plane strain three degrees of freedom: two translational degrees of freedom and one independent rotational degree of freedom (Fig. 3). The gradients of the rotation are connected to curvatures which are associated with couple stresses. It leads to a non-symmetry of the stress tensor and the presence of a characteristic length. The capability of a polar hypoplastic model has already been demonstrated in solving boundary value problems involving localization such as biaxial test, shearing of a narrow granular layer, silo filling and silo flow, furnace flow, footings and sand anchors. A close agreement between calculations and experiments was achieved. A polar model has good physical grounds since it takes into account rotations and couple stresses which are observed during shearing, but remain negligible during homogeneous deformation. A characteristic length is directly related to a mean grain diameter. However, the model is only suitable for shear dominated problems, but not for tension (decohesion) dominated applications.

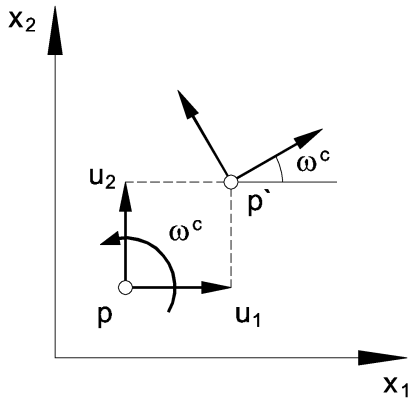

a)

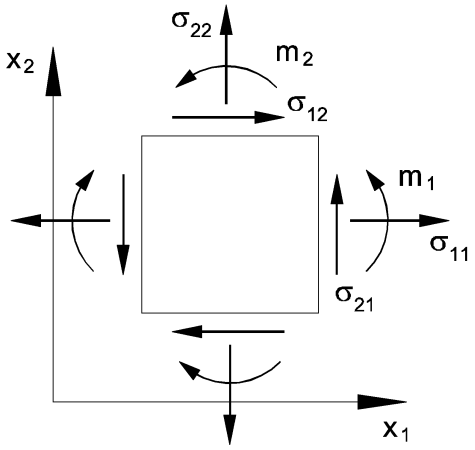

b)

Fig. 3. Plane strain Cosserat continuum: a) degrees of freedom (u_1 – horizontal displacement, u_2 – vertical displacement, ω^c – Cosserat rotation), b) stresses σ_{ij} and couple stresses m_i at an element

The constitutive law can be summarized for plane strain as follows (Tejchman 1997, Tejchman et al 1998, Tejchman and Gudehus 2001, Tejchman 2002, Huang and Bauer 2002, Nübel 2002, Tejchman and Bauer 2004) (Eqs. 2–4, 7–14, 16–18):

$$\overset{0}{\sigma}_{ij} = f_s \left[L_{ij} \left(\hat{\sigma}_{kl}, \hat{m}_k, d^c_{kl}, k_k d_{50} \right) + f_d N_{ij} \left(\hat{\sigma}_{ij} \right) \sqrt{d^c_{kl} d^c_{kl} + k_k k_k d^2_{50}} \right], \tag{18}$$

$$\overset{0}{m}_i / d_{50} = f_s \left[L^c_i \left(\hat{\sigma}_{kl}, \hat{m}_k, d^c_{kl}, k_k d_{50} \right) + f_d N^c_i \left(\hat{m}_i \right) \sqrt{d^c_{kl} d^c_{kl} + k_k k_k d^2_{50}} \right], \tag{19}$$

$$L_{ij} = a_1^2 d_{ij}^c + \hat{\sigma}_{ij} \left(\hat{\sigma}_{kl} d_{kl}^c + \hat{m}_k k_k d_{50} \right), \tag{20}$$

$$L_i^c = a_1^2 k_i d_{50} + a_1^2 \hat{m}_i \left(\hat{\sigma}_{kl} d_{kl}^c + \hat{m}_k k_k d_{50} \right), \tag{21}$$

$$N_{ij} = a_1 \left(\hat{\sigma}_{ij} + \hat{\sigma}_{ij}^* \right), \qquad N_i^c = a_1^2 a_c \hat{m}_i, \tag{22}$$

$$\overset{0}{m}_i = \dot{m}_i - 0.5 w_{ik} m_k + 0.5 m_k w_{ki}, \qquad \hat{m}_i = \frac{m_i}{\sigma_{kk} d_{50}} \tag{23}$$

$$d_{ij}^c = d_{ij} + w_{ij} - w_{ij}^c, \qquad k_i = w_{,i}^c, \tag{24}$$

$$w_{kk}^c = 0, \qquad w_{21}^c = -w_{12}^c = w^c, \tag{25}$$

wherein m_i – Cauchy couple stress vector, $\overset{0}{m}_i$ – Jaumann couple stress rate vector, d_{ij}^c – polar rate of deformation tensor, k_i – rate of curvature vector, w^c – rate of Cosserat rotation, d_{50} – mean grain diameter, a_c – micro-polar parameter. A micro-polar parameter can be correlated with the grain roughness. It was estimated with a numerical analysis for shearing of a narrow granular strip between two very rough boundaries as $a_c = a_1^{-1}$ (Tejchman 1997, Gudehus and Tejchman 2001). The polar hypoplastic law has totally 9 material constants (with a uniform distribution of the initial void ratio in the granular specimen).

4. Finite Element Data

FE-calculations of plane strain compression tests were performed with a sand specimen which was $h_0 = 10$ cm high and $b = 2$ cm wide. Only quadrilateral finite elements composed of four diagonally crossed triangles were applied to avoid volumetric locking. In all, 320 quadrilateral elements (0.25×0.25 cm) divided into 1280 triangular elements with linear shape functions for displacements were used. The dimensions of finite elements were $5 \times d_{50}$ to obtain the thickness of shear zones independent of the mesh size (Tejchman et al 1999, Maier 2002). The integration was performed with one sampling point placed in the middle of each element. The calculations were carried out with small deformations and curvatures.

As the initial stress state, the state with $\sigma_{22} = \sigma_c + \gamma_d x_2$ and $\sigma_{11} = \sigma_c$ was assumed in the sand specimen, where σ_c denotes the confining pressure ($\sigma_c = 0.2$ MPa), x_2 is the vertical coordinate measured from the top of the specimen, γ_d denotes the initial volume weight (σ_{11} – horizontal normal stress, σ_{22} – vertical normal stress).

A quasi-static deformation in sand was initiated through a constant vertical displacement increment prescribed at nodes along the upper edge of the specimen. The boundary conditions of the sand specimen were no shear stress at the top

and bottom. To preserve the stability of the specimen against the sliding along the bottom boundary, the node in the middle of the bottom was kept fixed.

To obtain a shear zone inside the granular specimen, single imperfections and imperfections distributed stochastically were assumed. The single imperfections were inserted into the specimen in the form of a weaker finite element (with a higher initial void ratio) or a stronger finite element (with a lower initial void ratio). The initial density of the entire specimen (besides imperfections) was low (dense specimen) and high (loose specimen). The number of imperfect elements changed from 1 to 3. The location and distance of imperfect elements varied. The imperfections were located symmetrically and non-symmetrically against the vertical axis of symmetry.

The effect of a distribution of the initial void ratio e_0 in the entire specimen was also investigated. In the first case, the initial void ratio e_0 was randomly distributed (by means of a random generator) in such a way that the initial void ratio was increased in every element layer by the value $a \times r$, where a is a constant (e.g. 0.0001, 0.05, 0.10) and r is a random number between 0 and 1. Thus, the fluctuating initial void ratio in an initially dense specimen was equal to

$$e_0 = 0.60 + 0.0001r \quad \text{or} \quad e_0 = 0.60 + 0.05r \quad \text{or} \quad e_0 = 0.60 + 0.10r. \tag{26}$$

In addition, the initial void ratio was distributed stochastically in the specimen with an exponential frequency function proposed by Shahinpoor (1981) (Nübel and Karcher 1998, Nübel 2002). According to Shahinpoor (1981), the theoretical probability density function (Fig. 4) for the frequency distribution of macroscopic void ratio e for equal spheres is

$$p(e) = \frac{\lambda \exp(-\lambda e)}{\exp(-\lambda e_m) - \exp(-\lambda e_M)}. \tag{27}$$

This function is of the negative exponential type (Fig. 4) and is based on the concept of the Voronoi cells. The range of possible void ratios is limited by e_m (the minimum void ratio) and e_M (the maximum void ratio). The probability density function between the bounds of e_m and e_M is normalized (Fig. 4):

$$\int_{e_m}^{e_M} p(e)de = 1. \tag{28}$$

The critical void ratio (Eq. 14) is equal to

$$e_c = 0.5(e_m + e_M). \tag{29}$$

The constant λ depends on the soil density and can be obtained from a given average void ratio $\bar{e}$ (Nübel 2002):

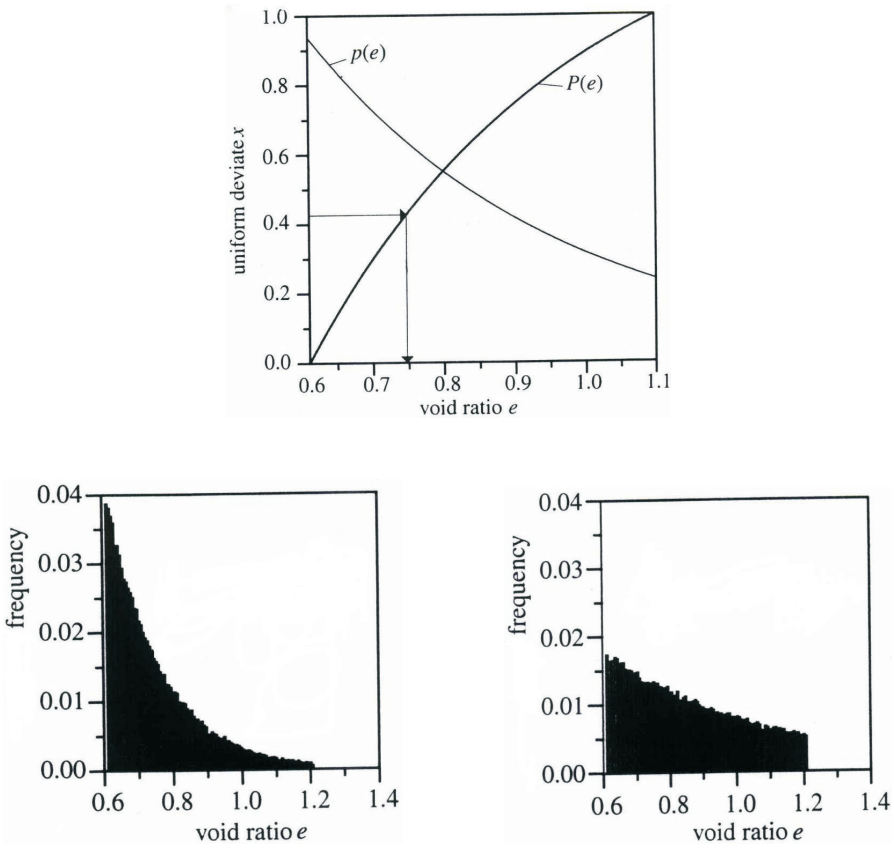

Fig. 4. Functions $p(e)$ and $P(e)$ and the distribution of local void ratio for two different mean global void ratios (Nübel and Karcher 1998)

$$\bar{e}_0 = \lambda^{-1} + \left(\frac{e_m \exp(-\lambda e_m) - e_M \exp(-\lambda e_M)}{\exp(-\lambda e_m) - \exp(-\lambda e_{M)}} \right). \tag{30}$$

Thus, for the average initial void ratio $\bar{e}_0 = 0.55$, the constant λ is equal to $\lambda = 1.34$, for $\bar{e}_0 = 0.60$, the constant $\lambda = 1.0$ and for $\bar{e}_0 = 0.65$, the constant $\lambda = 0.80$. The fluctuating initial void ratio e can be calculated by the formula

$$e = P^{-1}(x) = -\frac{1}{\lambda} \ln \left[(1 - r) \exp(-\lambda e_m) + r \exp(-\lambda e_M) \right], \tag{31}$$

with

$$P(e) = \int_{e_m}^{e_M} p(e) de. \tag{32}$$

The parameter r is the random number chosen between 0 and 1. The deviation of the distribution of void ratio increases with decreasing number of voids (grains) in a volume element and decreasing mean global void ratio of the specimen (Fig. 4).

For the solution of a non-linear system, a modified Newton-Raphson scheme with line search was used with a global stiffness matrix calculated with only first terms of the constitutive equations (linear in d^c_{kl} and $\kappa_k d_{50}$). The stiffness matrix was updated every 100 steps. To accelerate the calculations in the softening regime, the initial increments of displacements and Cosserat rotation in each calculation step were assumed to be equal to the final increments in the previous step (Tejchman 1997). The iteration steps were performed using translational and rotational convergence criteria (Tejchman 1997). For the time integration of stresses in finite elements, a one-step Euler forward scheme was applied.

5. Numerical Results

5.1. Single Imperfections

5.1.1. Initially Dense Specimen

Figs. 5–7 present the results with an initially dense specimen ($e_0 = 0.60$) including one single weaker element ($e_0 = 0.65$) at mid-point along the left side. The normalized load-displacement curve is depicted in Fig. 5. Figure 6 shows the deformed FE-mesh with the distribution of the Cosserat rotation ω^c and couple stress m_1 near the peak state. The deformed FE-mesh with the distribution of Cosserat rotation ω^c, void ratio e, stress σ_{12} and couple stress m_1 at residual state is demonstrated in Fig. 7. The magnitude of the Cosserat rotation is marked by circles with a maximum diameter corresponding to the maximum rotation in the given step. In turn, the darker the region, the higher the void ratio. The entire range of Cosserat rotation and void ratio was divided into 10 different circle sizes and shadows. The displacements shown were magnified with regard to the calculated ones by the factor of about 3.

The resultant vertical force on the specimen top P increases first, shows a pronounced peak, drops later and reaches an almost a residual state (Fig. 5). The overall angle of internal friction for the sand specimen, calculated from Mohr's formula

$$\phi = \arcsin \frac{\sigma_1 - \sigma_2}{\sigma_1 + \sigma_2}, \tag{33}$$

is equal to $\phi_p = 43.5^\circ$ at peak ($u/h_0 = 2.64\%$). At $u/h_0 = 10\%$, it is equal to $\phi_{cr} = 34.0^\circ$. In Eq. 33, $\sigma_1 = P/(bl)$ denotes the vertical principle stress ($\sigma_2 = \sigma_c = 0.2$ MPa is the horizontal principal stress, $b = 0.02$ m is the specimen width, $l = 1.0$ m and u dotes the vertical displacement of the top).

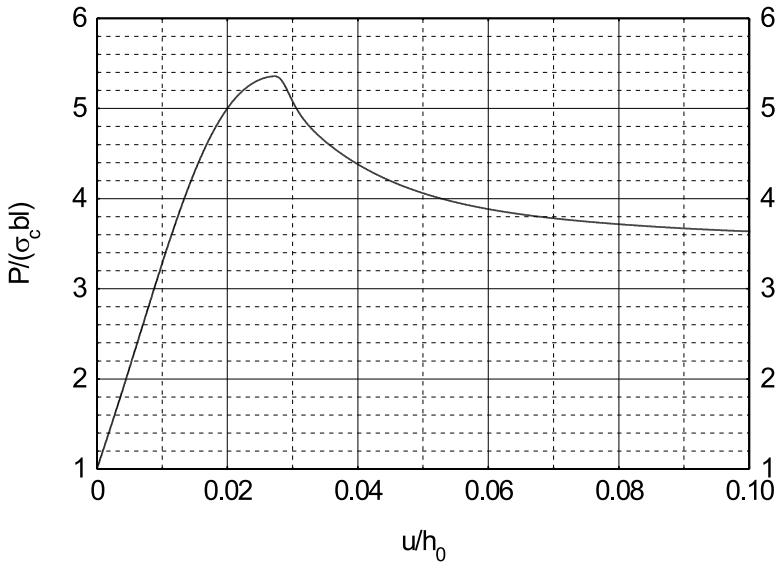

Fig. 5. Load-displacement curve ($e_0 = 0.60$, one weaker spot)

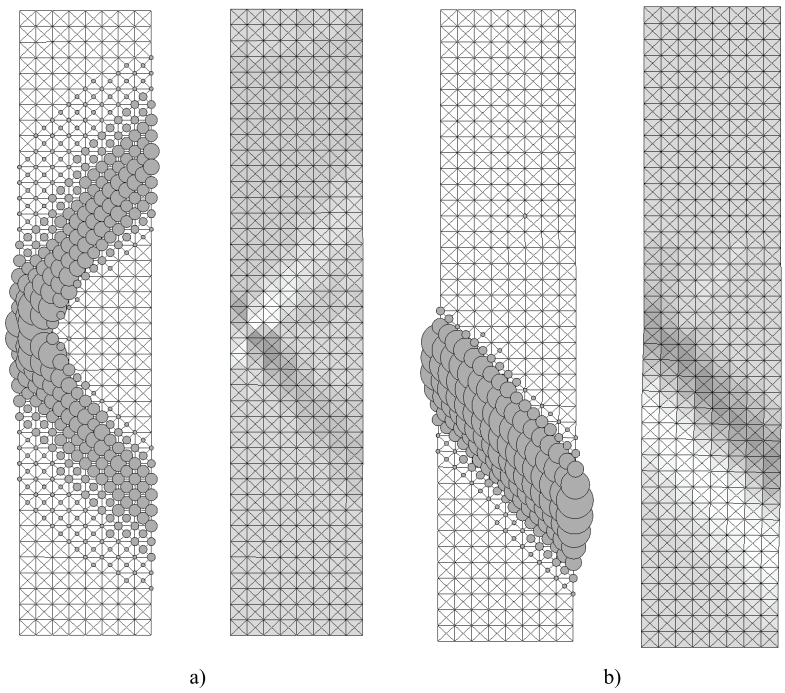

Fig. 6. Deformed FE-mesh with the distribution of Cosserat rotation ω^c and couple stress m_1 at $u/h_0 = 2.5\%$ (a) and at $u/h_0 = 3.0\%$ (b) ($e_0 = 0.60$, one weaker spot)

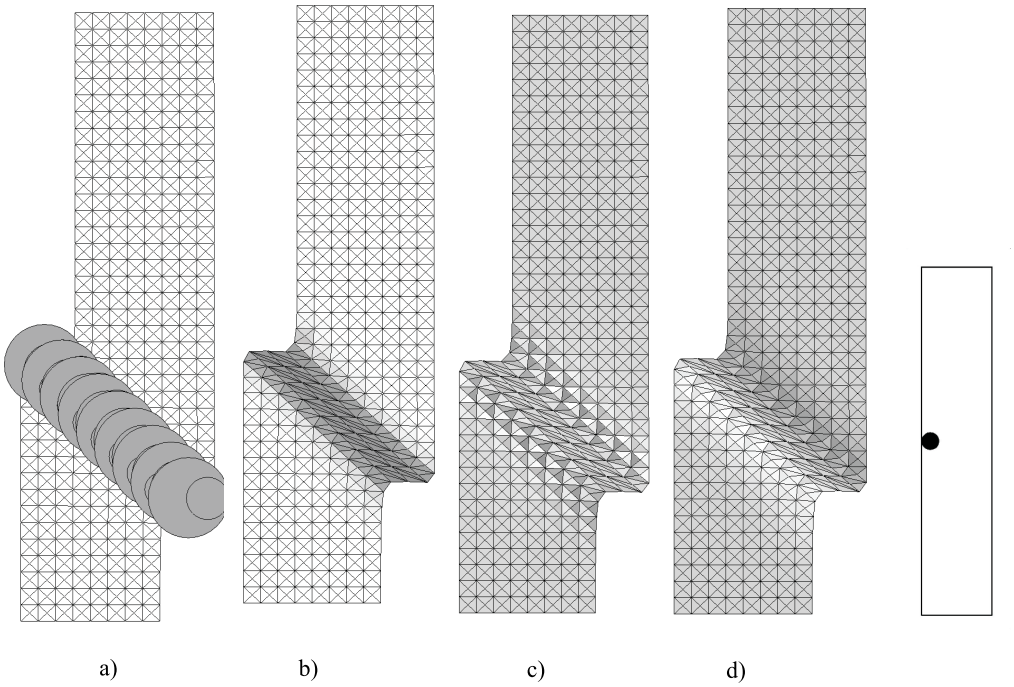

Fig. 7. Deformed FE-mesh with the distribution of Cosserat rotation ω^c (a), void ratio e (b), shear stress σ_{12} (c) and couple stress m_1 (d) at residual state $u/h_0 = 10\%$ ($e_0 = 0.60$, one weaker spot)

The obtained results of internal friction angles at peak and in the residual state in dense sand, and the corresponding vertical displacements of the sand specimen compare well with experimental results with Karlsruhe sand carried out by Vardoulakis (1977, 1980) and Yoshida et al (1994). In the experiments by Vardoulakis (1977, 1980), the dimension of the specimen were: $h_0 = 140$ mm, $b = 40$ mm, $l = 80$ mm and in the experiments by Yoshida et al (1994): $h_0 = 200$ mm, $b = 80$ mm, $l = 160$ mm, respectively. In the biaxial apparatus by Vardoulakis (1977), the top surface of the specimen was in contact with a lubricated polished stainless steel cap. The bottom of the specimen was located on a roller bearing. Both top and bottom surfaces in the biaxial apparatus by Yoshida et al (1994) were in contact with lubricated polished stainless steel cap and pedestal. The experiments with very dense sand ($e_0 = 0.55$) resulted in $\phi_p = 45.7^{\circ}$ and $\phi_{cr} = 32.9^{\circ}$ (Vardoulakis 1977, 1980), and $\phi_p = 43.4^{\circ}$, and $\phi_{cr} = 31.3^{\circ}$ (Yoshida et al 1994) at $\sigma_c = 200$ kPa.

At the beginning of the displacement of the top boundary, two shear zones are created expanding outwards from the weakest element towards the top and bottom of the specimen (Fig. 6a). Afterwards, one of the shear zones becomes inactive (slightly before the peak state, Tejchman 2003b) and only one shear zone starts to form. It is characterized both by a concentration of shear deformations,

couple stresses and Cosserat rotation, and a significant increase of the void ratio (Fig. 7). The thickness of the internal shear zone is approximately $t_{sz} \cong 12 \times d_{50}$. The calculated thickness is in accordance with the observed thickness during experiments with dense Karlsruhe sand at $\sigma_c = 200$ kPa: $t_{sz} = 13 \times d_{50}$ (Vardoulakis 1977, 1980) and $10 \times d_{50}$ (Yoshida et al 1994). The calculated maximum Cosserat rotation in the middle of the shear zone is 1.4 at $u/h_0 = 10\%$.

Fig. 8 shows results for a initially dense specimen ($e_0 = 0.60$) including one stronger element ($e_0 = 0.55$) located at mid-point of the left side. At the beginning of the compression process, two shear zones are created expanding outward from the imperfection, (similarly as in the case of a weaker spot). Afterwards, they become passive. The new shear zone occurs in the lower part of the right side of the specimen. It propagates towards the bottom and is reflected from the fixed bottom (Tejchman 2002).

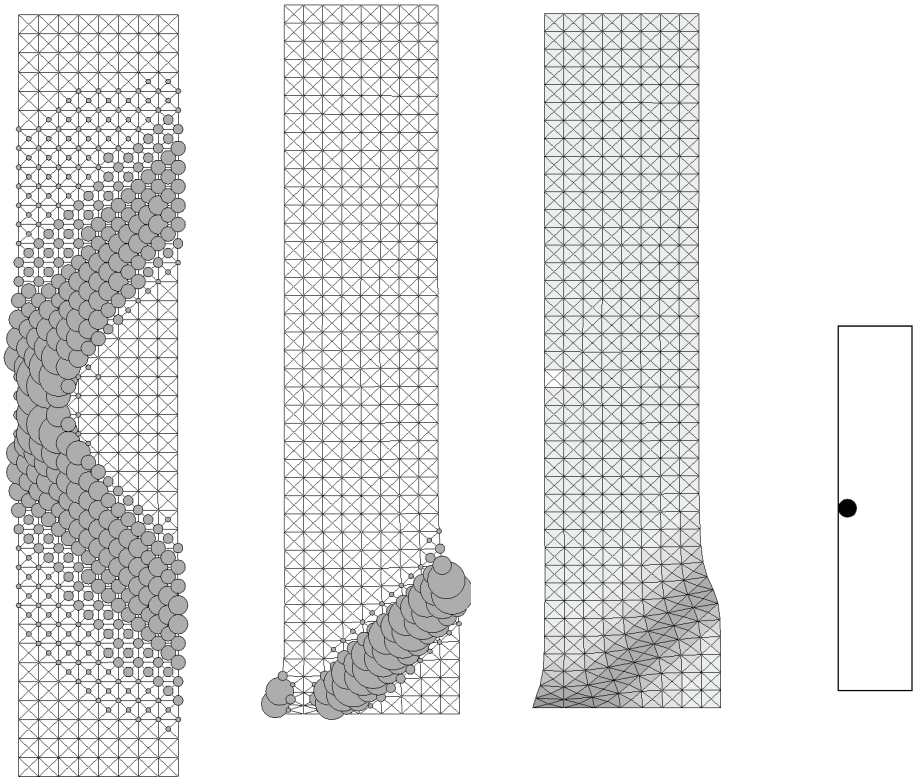

Fig. 8. Deformed FE-mesh with the distribution of Cosserat rotation ω^c at $u/h_0 = 2.5\%$ (a) and $u/h_0 = 5\%$ (b) and void ratio e at $u/h_0 = 5\%$ (c) ($e_0 = 0.60$, one stronger spot)

The effect of the spacing of weaker elements in the dense specimen are demonstrated in Figs. 9–10. Three weak elements ($e_0 = 0.90$) are located uniformly along

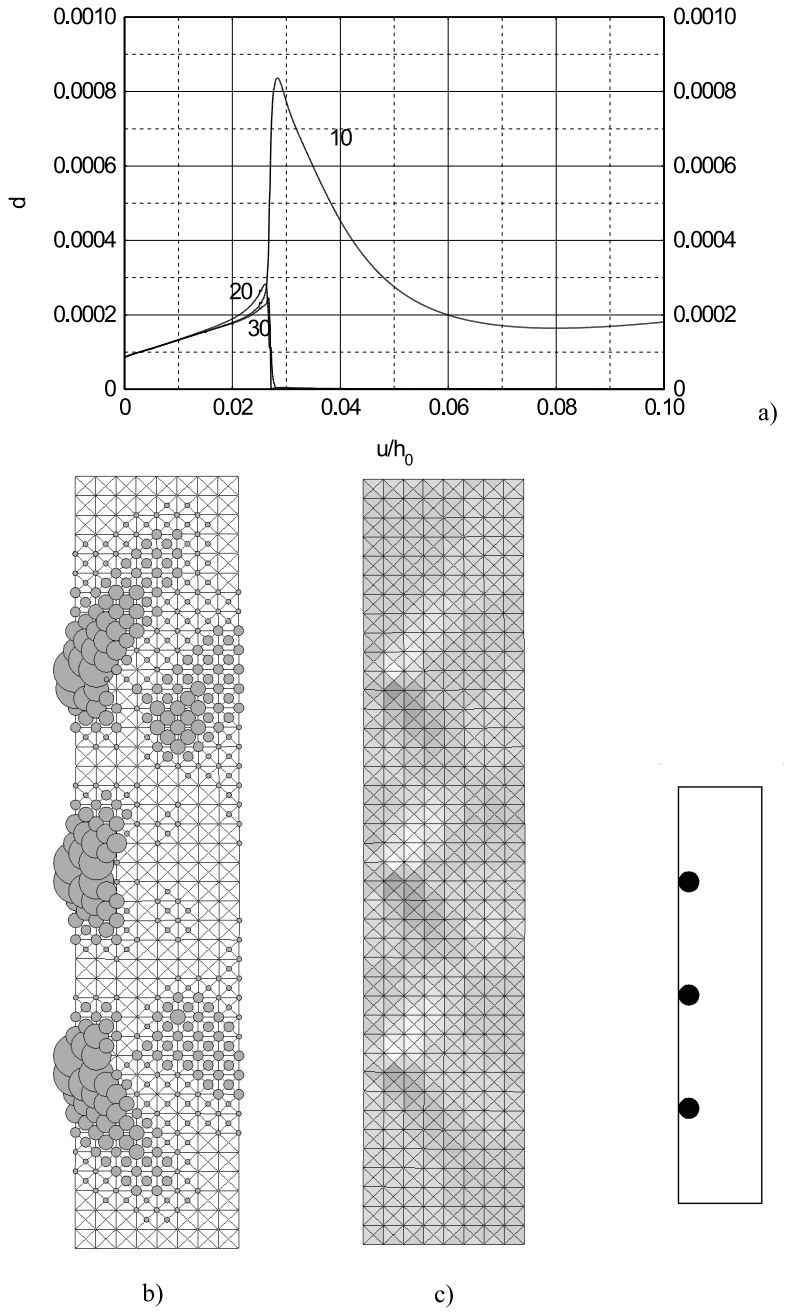

Fig. 9. Evolution of modulus of the deformation rate $\sqrt{d^c_{kl}d^c_{kl} + k_k k_k d^2_{50}}$ in weaker elements along the left side (a), and deformed FE-mesh with the distribution of Cosserat rotation ω^c (b) and couple stress m_1 (c) at $u/h_0 = 2.5\%$, and Cosserat rotation ω^c (d), void ratio e (e) and couple stress m_1 (f) at $u/h_0 = 10\%$ ($e_0 = 0.60$, three weaker spots at distance of 25 mm, '10' – the lowest spot, '30' – the highest spot)

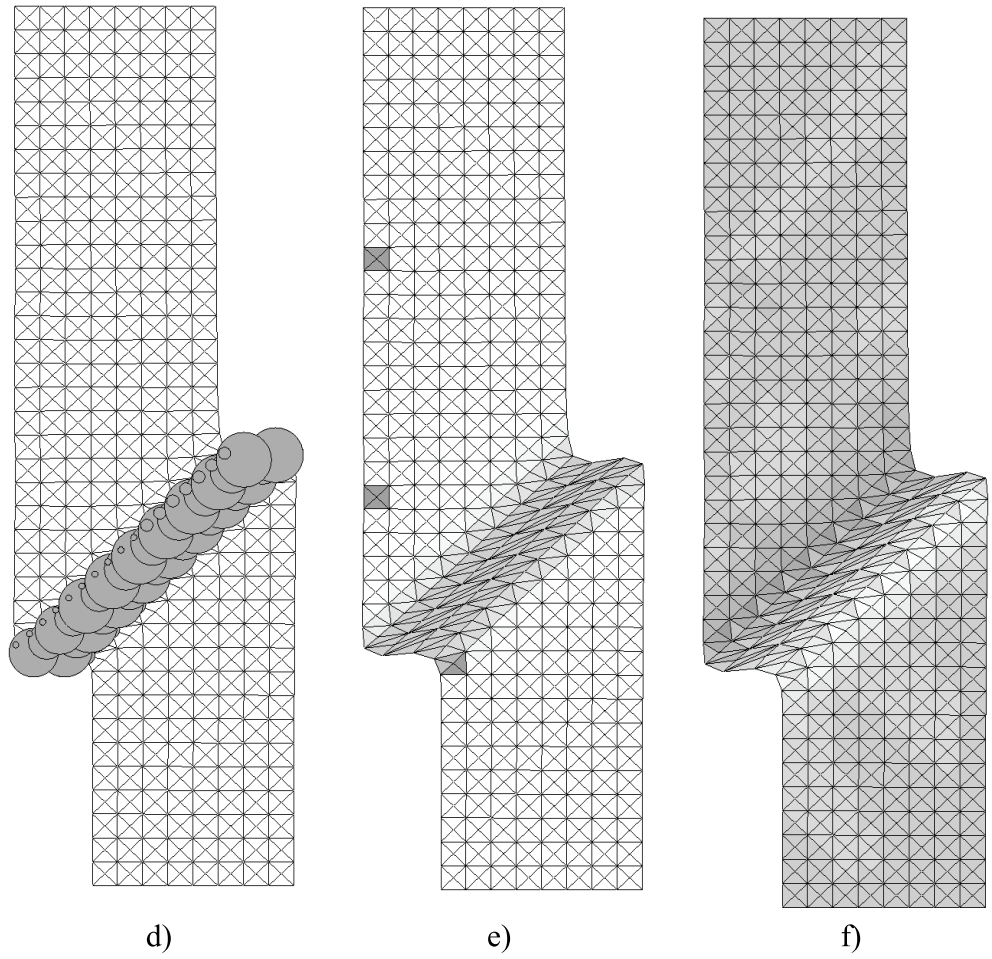

Fig. 9. Cont.

the left side of the specimen at distances of about 25 mm (Fig. 9) and 2.5 mm (Fig. 10). In the case of their distance of 25 mm, at the beginning, two shear zones are always created expanding outward from each weaker element. Afterwards and up to the end, only one shear zone dominates (starting from the lowest weaker spot). It forms intensively between $u/h_0 = 2.25\%$ and $u/h_0 = 2.84\%$ on the basis of the evolution of the modulus of deformation rate $\sqrt{d^c_{kl} d^c_{kl} + k_k k_k d^2_{50}}$ (Eqs. 18 and 19), Fig. 9a. The peak on the load-displacement curve takes place at $u/h_0 = 2.64\%$. The remaining shear zones start to become passive at the beginning of intense shearing in the dominated shear zone i.e. at $u/h_0 = 2.25\%$ (Fig. 9). They are 'dead' slightly after the peak state at $u/h_0 = 2.67\%$. The thickness of the shear zone is the same as in the case of one weaker spot (Figs. 6 and 7). However, the direction of propagation is different.

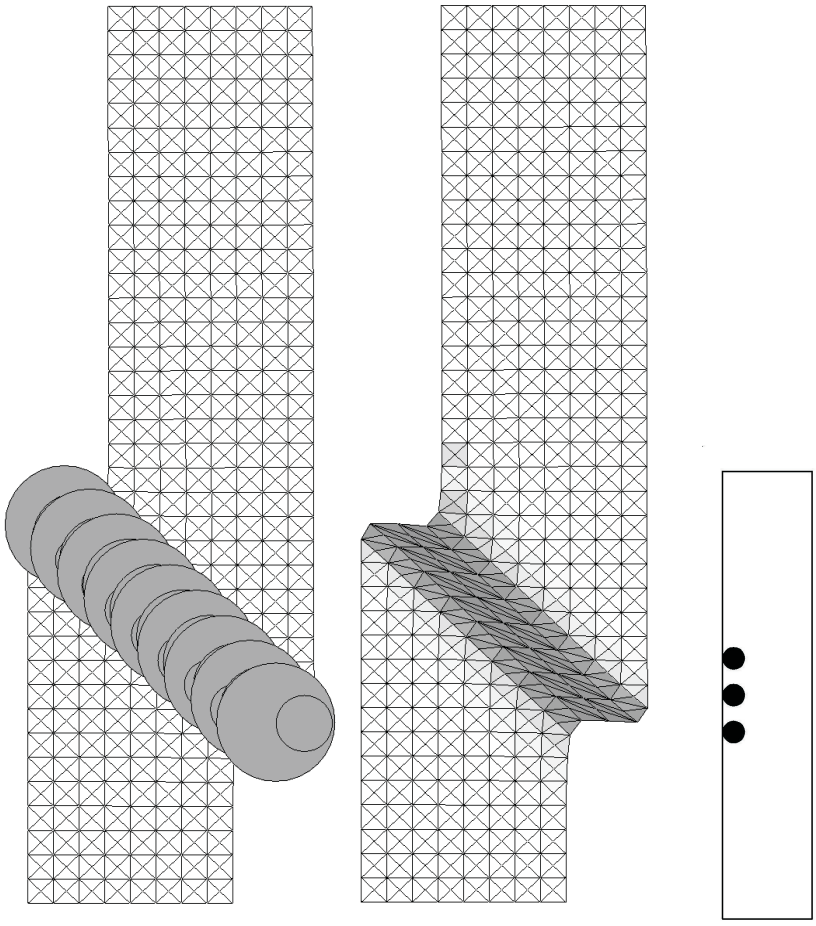

Fig. 10. Deformed FE-mesh with the distribution of Cosserat rotation ω^c (a) and void ratio e (b) at $u/h_0 = 10\%$ (b) ($e_0 = 0.60$, three weaker spots at distance of 2.5 mm)

If the weaker elements are very close to each other (Fig. 10), the shear zone is created at the same place as in the case of one weaker spot (Figs. 6 and 7). The direction of the propagation is also the same. In contrast to FE-calculations of simple shearing of an infinite granular layer (Shi and Chang 2003), the thickness of the shear zone does not grow and is always the same (irrespective of the spacing of weaker spots).

Fig. 11 shows the results with three stronger spots located along the left side at a distance of 2.5 mm (Fig. 11a) and with two weaker spots located symmetrically at mid-point of the left and right sides (Fig. 11b). Similarly as during calculations with one stronger spot, the location of the shear zone is different from that of initial stronger spots (Fig. 11a). In the case of two symmetric weaker spots, the

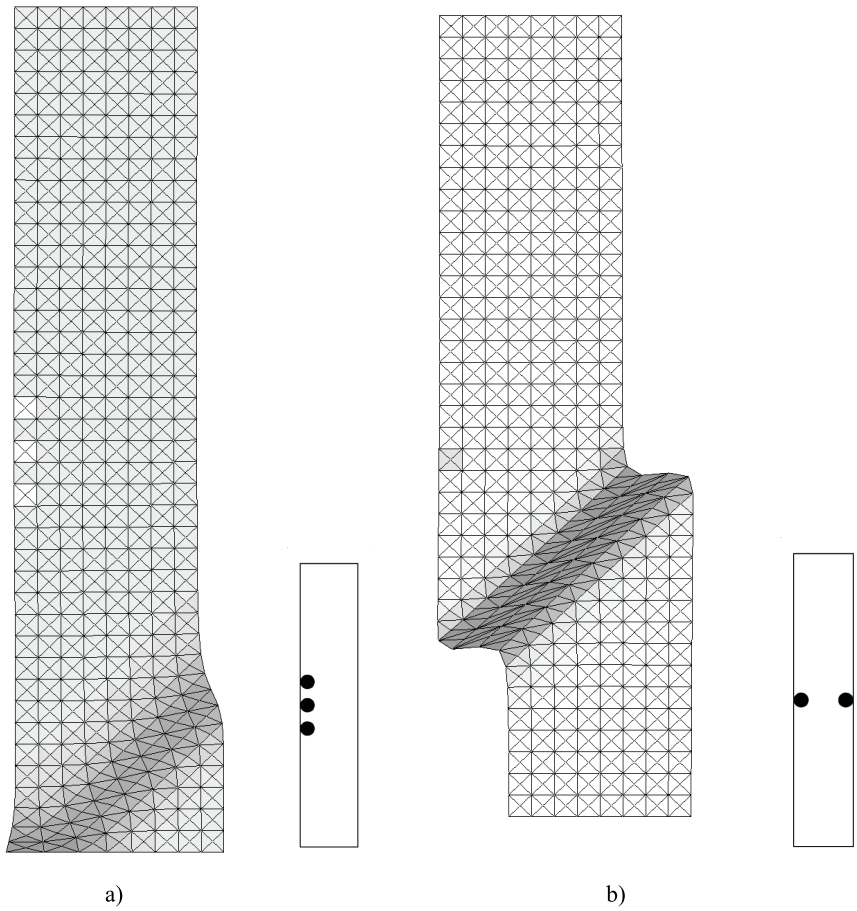

Fig. 11. Deformed FE-mesh with the distribution of void ratio e at residual state ($e_0 = 0.60$): a) three stronger spots located along the left side, b) two weaker spots located at mid-point of the left and right side

location of the shear zone is always connected to the location of one of the initial spots (Fig. 11b).

5.1.2. Initially Loose Specimen

In Figs. 12–14, the results with an initially loose specimen ($e_0 = 0.90$) are presented. The specimen includes one stronger spot ($e_0 = 0.65$), one weaker spot ($e_0 = 1.1$) at mid-point of the left side or three stronger spots ($e_0 = 0.65$) located along the left side at distances of 25 mm.

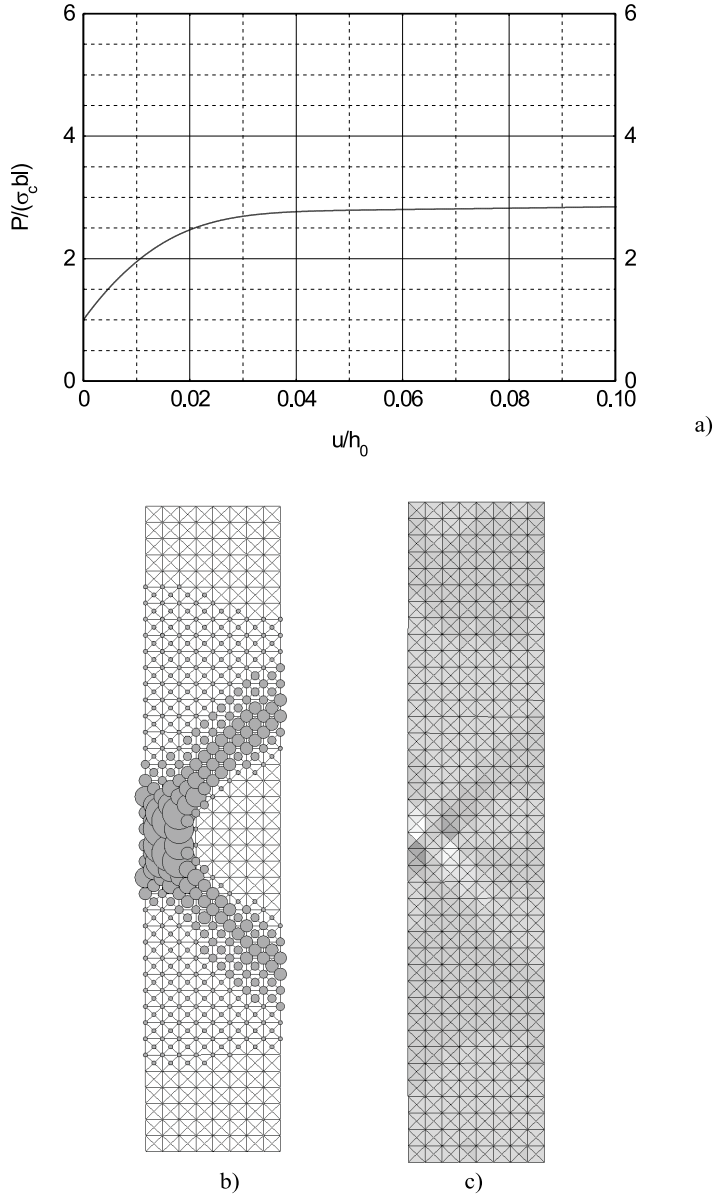

Fig. 12. Load-displacement curve (a), deformed FE-mesh with the distribution of Cosserat rotation ω^c (b) and couple stress m_1 (c) at $u/h_0 = 2.5\%$, and Cosserat rotation ω^c (d), void ratio e (e) and couple stress m_1 (f) at $u/h_0 = 10\%$ (c) ($e_0 = 0.90$, one stronger spot)

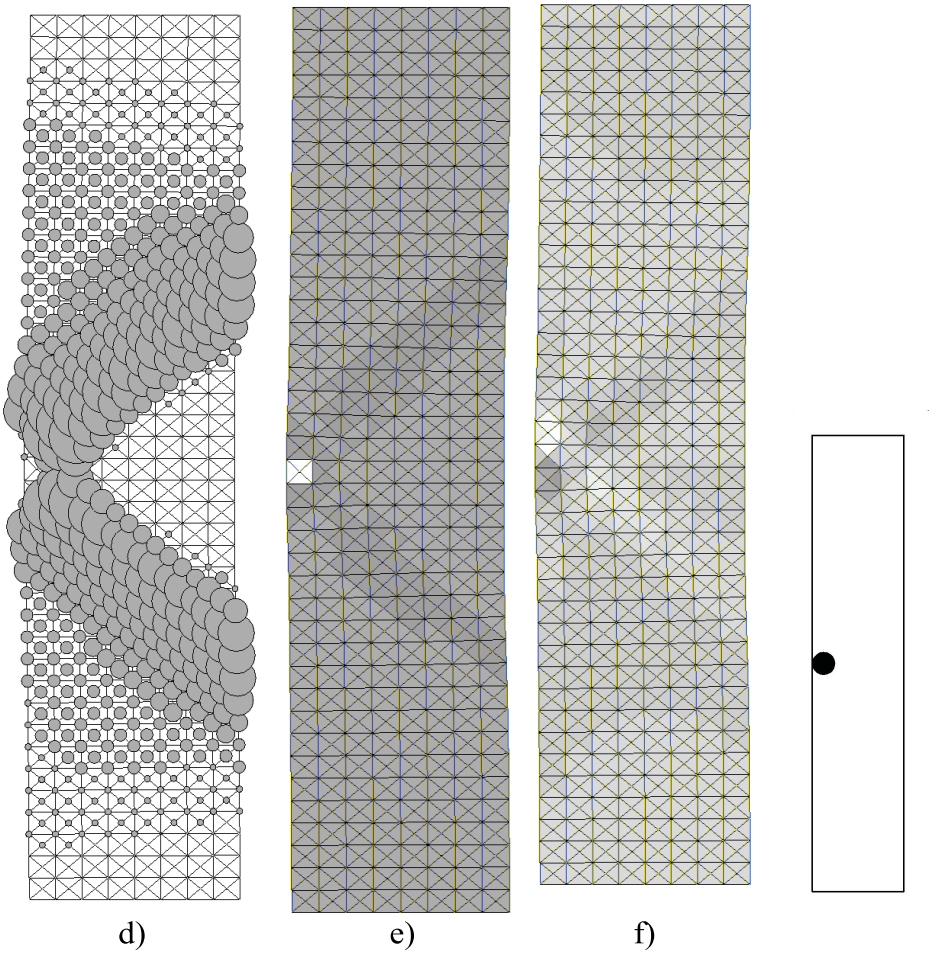

Fig. 12. Cont.

The normalized vertical force on the top continuously increases (Fig. 12a). The material experiences only contractancy (volume decrease). The overall angle of internal friction for the sand specimen, calculated from Mohr's formula (Eq. 34) is equal to 28.5° at $u/h_0 = 10\%$. At the beginning of loading, shear localizations always become active at each spot. However, since the specimen does not undergo material softening, all initial shear zones become inactive during further compression.

5.2. Random Distribution of Initial Void Ratio

Figs. 15–17 depict the results with a random distribution of the initial void ratio in the dense specimen (Eq. 27): $e_0 = 0.60 + 0.0001r$, $e_0 = 0.60 + 0.05r$ and $e_0 = 0.60 + 0.1r$ (a = 0.0001, 0.05, 0.1).

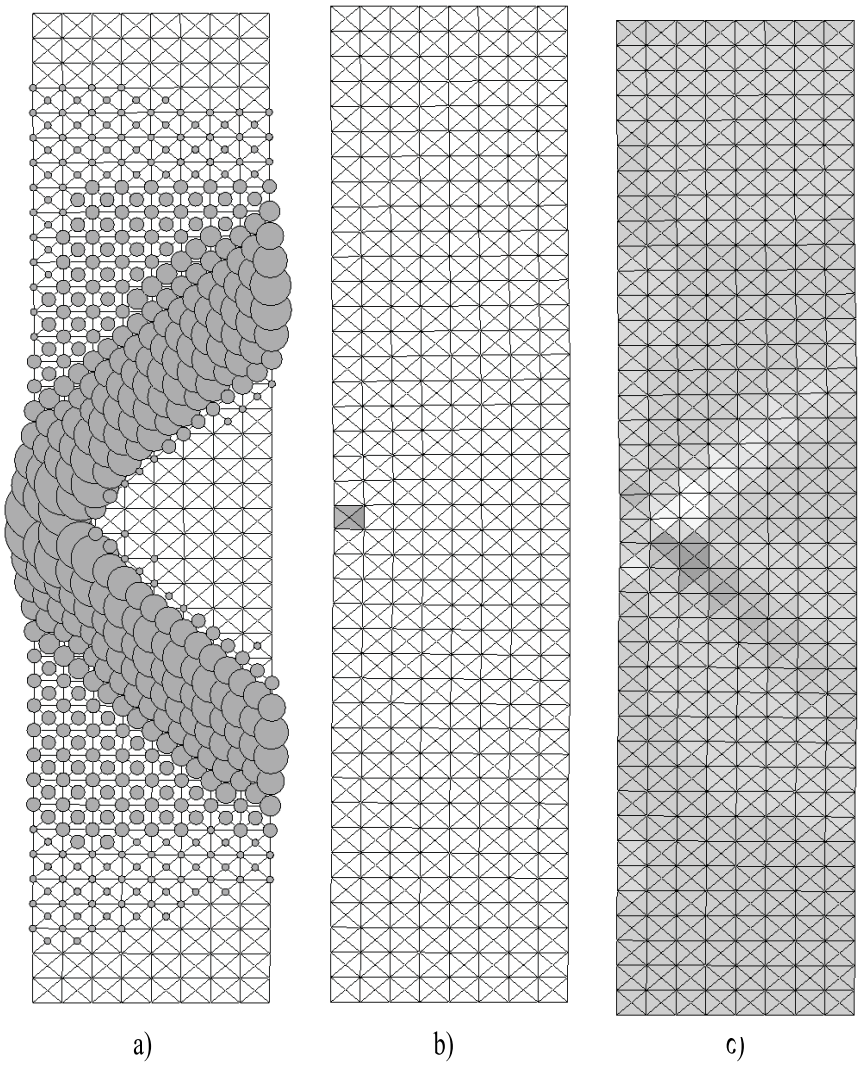

Fig. 13. Deformed FE-mesh with the distribution of Cosserat rotation ω^c (a), void ratio e (b) and couple stress m_1 (c) at $u/h_0 = 10\%$ ($e_0 = 0.90$, one weaker spot)

The maximum normalized vertical force on the top decreases with increasing constant a (Fig. 15) since the average initial void ratio e_0 increases. In turn, the residual force is slightly influenced. The location of shear localization strongly depends on the random distribution of e_0. It can be created in every region of the specimen (Fig. 16). When it is created in the lower or upper part of the specimen, it is reflected from the fixed bottom or moving top boundary. The thickness of the shear zone increases with decreasing rate of softening corresponding to a higher mean initial void ratio (Tejchman et al 1999, Tejchman 2003b). The smaller rate of softening after the peak state is connected to the lower material stiffness.

Thus, the larger deformation can develop. The calculated thickness of the internal shear zone is approximately $t_{sz} \cong 12 \times d_{50}$ ($e_0 = 0.60 + 0.0001r$), $t_{sz} \cong 15 \times d_{50}$ ($e_0 = 0.60 + 0.05r$) and $t_{sz} \cong 18 \times d_{50}$ ($e_0 = 0.60 + 0.1r$).

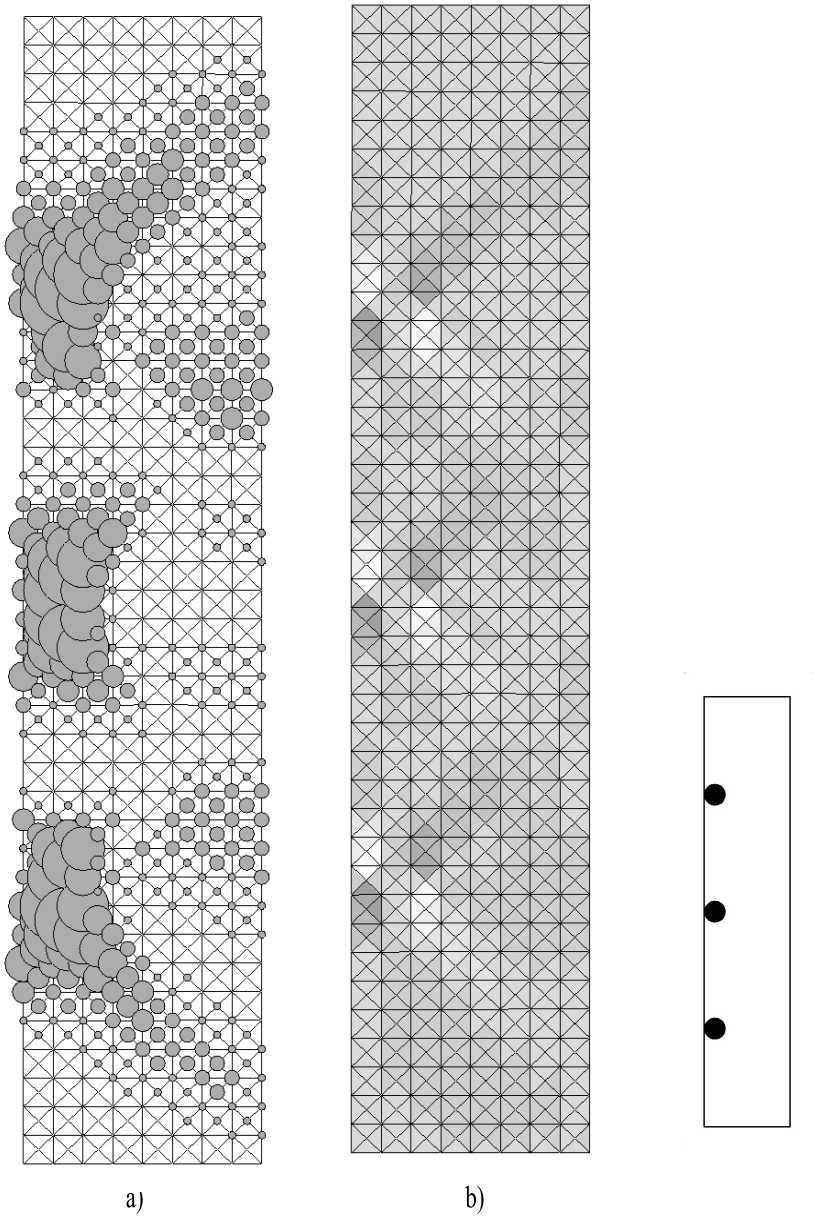

Fig. 14. Deformed FE-mesh with the distribution of Cosserat rotation ω^c (a) and couple stress m_1 (b) at $u/h_0 = 2.5\%$, and Cosserat rotation ω^c (c), void ratio e (d) and couple stress m_1 (e) at $u/h_0 = 10\%$ ($e_0 = 0.90$, three stronger spots at distance of 25 mm)

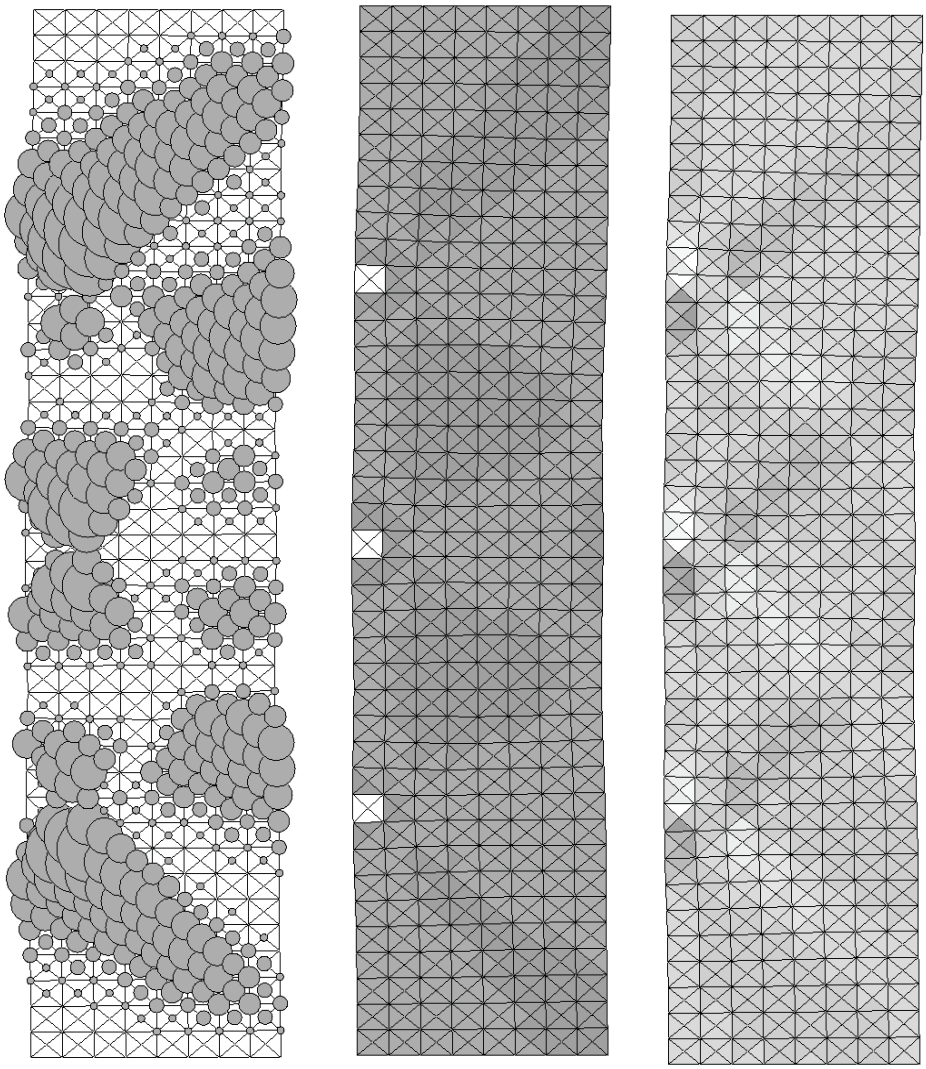

Fig. 14. Cont.

At an early stage of loading before the peak state, multiple shear zones appear (which are not well developed), Fig. 17. This numerical finding is in good agreement with experimental observations by Yoshida et al 1994. It is, however, in contrast with results of FE-calculations performed by Hobbs and Ord (1989) where the patterning of shear zones at residual state was obtained.

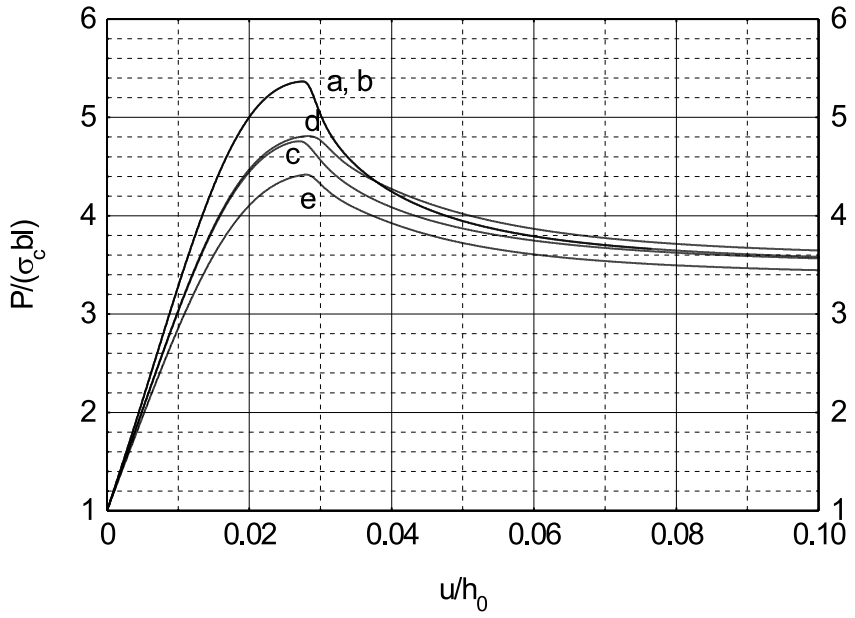

Fig. 15. Load-displacement curves with a random distribution of the initial void ratio: a) and b) $e_0 = 0.60 + 0.0001r$, c) and d) $e_0 = 0.60 + 0.05r$, e) $e_0 = 0.60 + 0.1r$

5.3. Stochastic Distribution of Initial Void Ratio

The FE-results with a stochastic distribution of the initial void ratio in dense specimens by Eq. 33 are shown in Figs. 18 and 19. One assumed $e_m = 0.001$ and $e_M = 1.641$. The parameter λ was 0.8 ($\bar{e}_0 = 0.65$), 1.0 ($\bar{e}_0 = 0.60$) and 1.34 ($\bar{e}_0 = 0.55$). Since the area of each finite element was $5d_{50} \times 5d_{50}$, the initial void ratio in each element was assumed to be the mean value of 25 random values calculated by Eq. 32. The void ratio scattering in dense specimens was limited by the pressure dependent void ratios e_{d0} and e_{c0}.

The maximum vertical force on the top boundary increases with decreasing mean global initial void ratio $\bar{e}_0$ (it is strongly affected by $\bar{e}_0$). The residual one is only slightly influenced. As in the case of a random distribution of the initial void ratio, the shear zone can propagate at different parts of the granular specimen. The thickness of the shear zone slightly increases with increasing mean void ratio $\bar{e}_0$. Thus, this increase is significantly smaller as compared with the calculations with a random distribution of the initial void ratio. The thickness of the shear zone with $\bar{e}_0 = 0.60$ is close to this with a random distribution of the initial void ratio at $a = 0.0001$. At an early stage of loading before the peak state, multiple shear zones are always created.

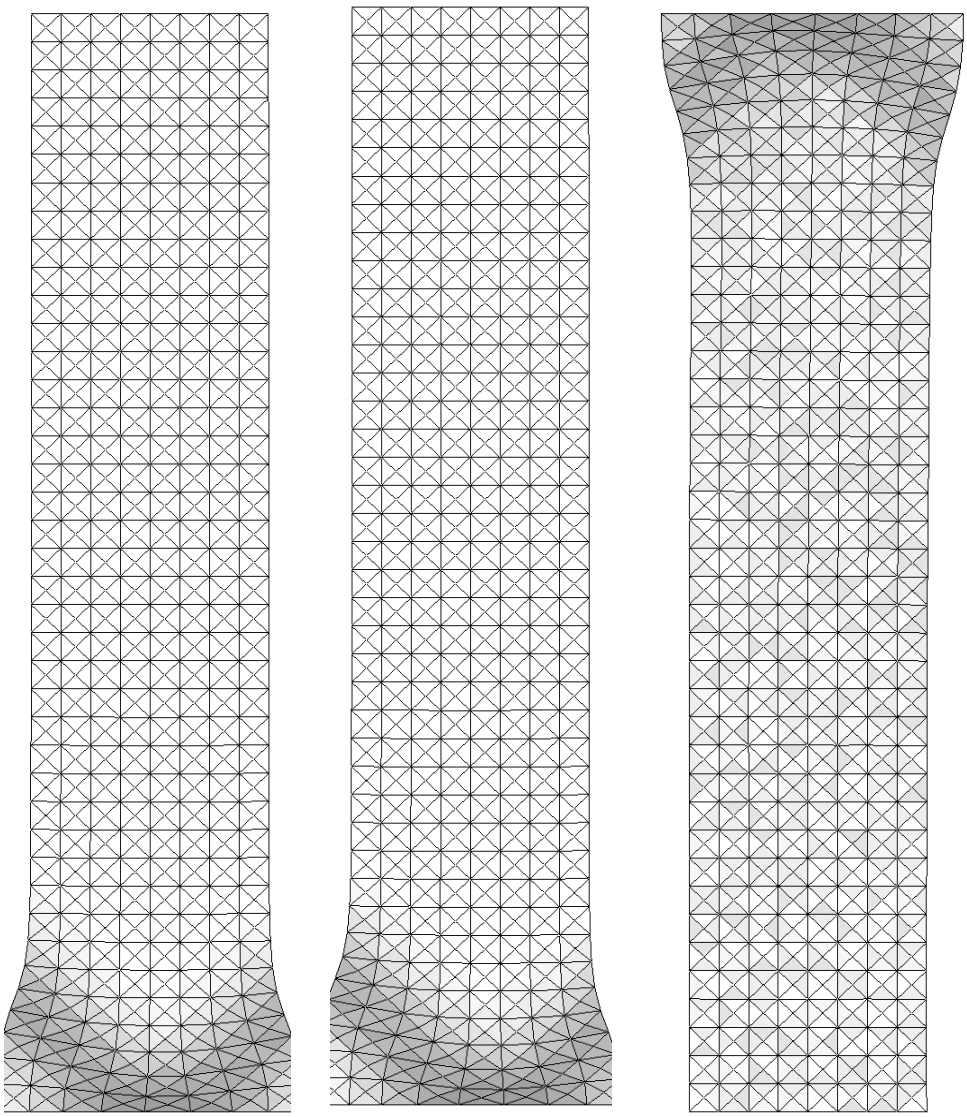

Fig. 16. Deformed FE-mesh with a distribution of void ratio at residual state: a) and b) $e_0 = 0.60+0.0001\ r$, c) and d) $e_0 = 0.60+0.05\ r$, e) $e_0 = 0.60+0.1\ r$

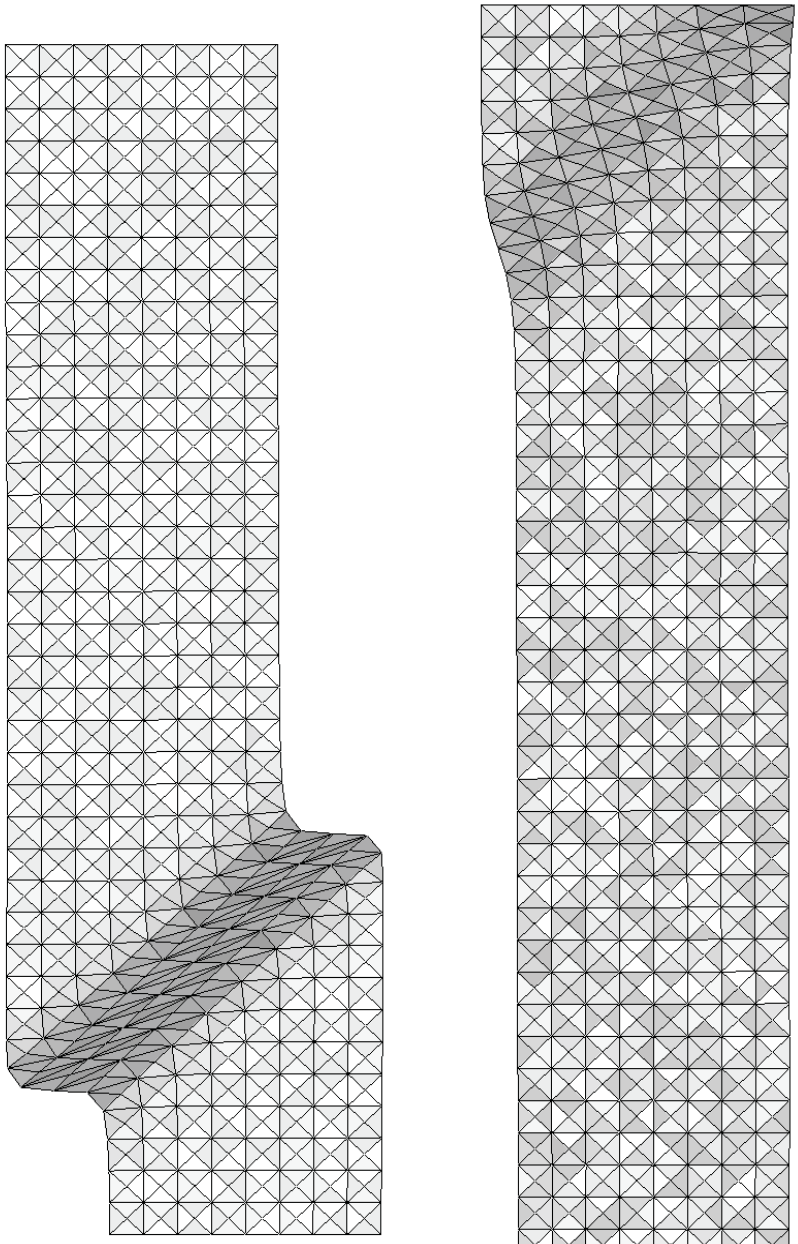

Fig. 16. Cont.

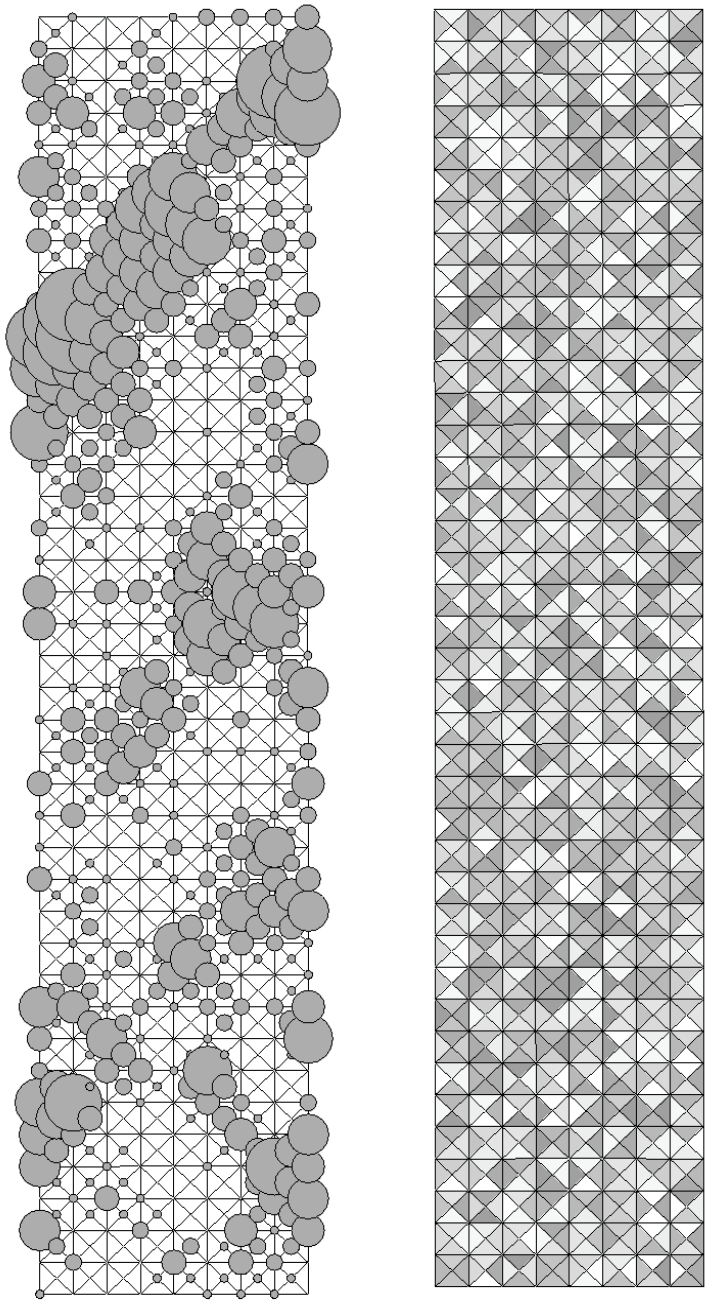

Fig. 17. Deformed FE-mesh with a distribution of Cosserat rotation and void ratio at $u/h_0 = 2.5\%$ ($e_0 = 0.60 + 0.05r$)

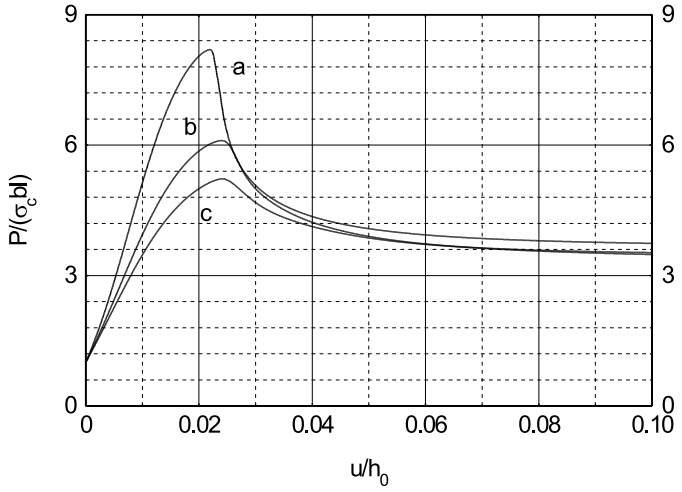

Fig. 18. Load-displacement curves with an exponential frequency distribution of the initial void ratio: (a) $\bar{e}_0 = 0.55$, (b) $\bar{e}_0 = 0.60$, (c) $\bar{e}_0 = 0.65$

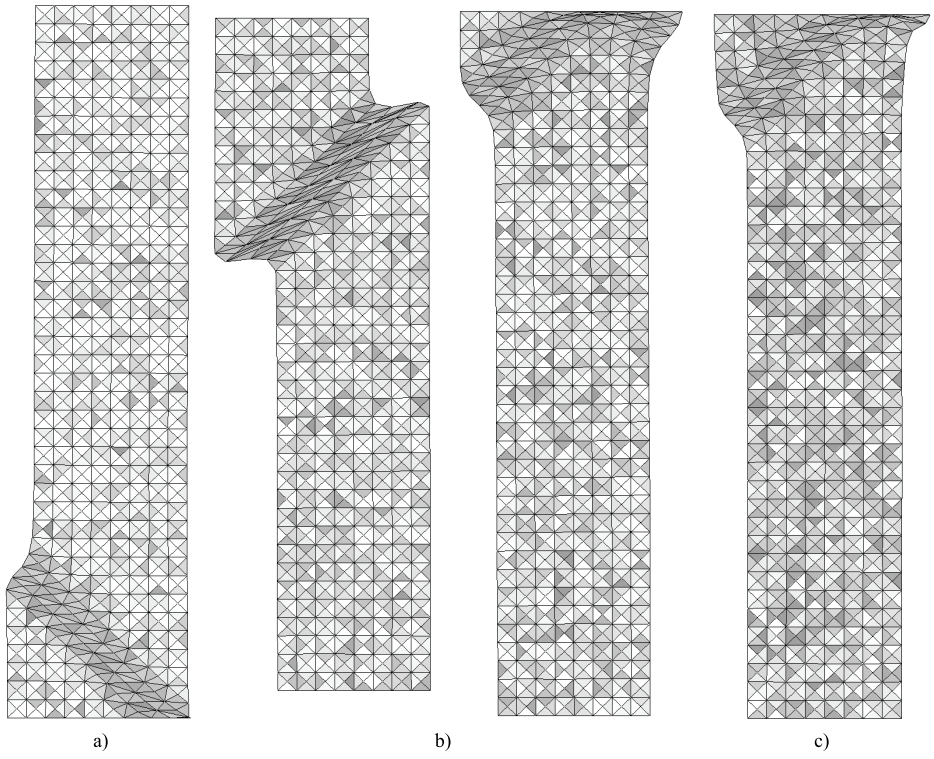

Fig. 19. Deformed FE-mesh with a distribution of void ratio at residual state (exponential frequency distribution of the initial void ratio): (a) $\bar{e}_0 = 0.55$, (b) $\bar{e}_0 = 0.60$, (c) $\bar{e}_0 = 0.65$

6. Conclusions

The following conclusions can be drawn on the basis of the performed FE-simulations on the effect of imperfections on shear localization during plane strain compression with a polar hypoplastic model:

- Each single imperfection (weaker and stronger spot) induces shear zones at the beginning of loading irrespective of the initial density of the specimen. Thus, multiple shear zones appear which are not well developed.
- The dominant single shear zone starts to form intensively in the dense specimen slightly before the peak state. It is well developed after the peak state.
- The dominant shear zone is connected to a weaker but not to a stronger spot.
- The spacing of single imperfections does not influence the thickness of the shear zone. However, it can influence the direction of the propagation.
- The distribution of the initial void ratio strongly influences the load-displacement diagram. It influences the thickness of the shear zone insignificantly if the mean global initial void ratio is approximately the same.
- The distribution of the initial void ratio strongly influences the location of the shear zone and its propagation direction. The shear zone can be created in every region of the dense specimen.
- The shear zone can reflect from fixed or moving rigid boundaries.
- The results with a random distribution of the initial void ratio are similar to those with a stochastic distribution using an exponential frequency function. However, in the case of a stochastic distribution of the initial void ratio, the effect of the changing average initial void ratio on the thickness of the shear zone is smaller.

References

Aifantis E. C. (1984), On the Microstructural Origin of Certain Inelastic Models, *J. Eng. Mater. Technol.*, 106, 326–334.

Bauer E. (1996), Calibration of a Comprehensive Hypoplastic Model for Granular Materials, *Soils and Foundations*, 36, 1, 13–26.

Bauer E. (2000), Conditions of Embedding Casagrande's Critical States into Hypoplasticity, *Mechanics of Cohesive-Frictional Materials*, 5, 125–148.

Bazant Z., Lin, F. B. (1988), Nonlocal Yield Limit Degradation, *Int. J. Num. Meth. Eng.*, 26, 1805–1823.

Belytschko T., Chiang H., Plaskacz E. (1994), High Resolution Two Dimensional Shear Band Computations: Imperfections and Mesh Dependence, *Com. Meth. Appl. Mech. Engng.*, 119, 1–15.

de Borst R. (1991), Simulation of Strain Localization: a Reappraisal of the Cosserat Continuum, *Engng. Computations*, 8, 317–332.

de Borst R., Mühlhaus H. B., Pamin J., Sluys L. Y. (1992), Computational Modelling of Localization of Deformation, *Proc. of the 3rd Int. Conf. Comp. Plasticity* (D. R. J. Owen, D. R. J. Onate, E., Hinton, eds.), Pineridge Press, Swansea, 483–508.

Brinkgreve R. (1994), Geomaterial Models and Numerical Analysis of Softening, *PhD Thesis*, Delft University, 1–153.

Chambon R., Caillerie D., El Hassan N. (1998), One-Dimensional Localization Studied with a Second Grade Model, *European Journal of Mechanics*, 17, 4, 637–656.

Desrues J., Chambon R., Mokni M., Mazerolle F. (1996), Void Ratio Evolution inside Shear Bands in Triaxial Sand Specimens Studied by Computed Tomography, *Géotechnique*, 46, 3, 529–546.

Gudehus G. (1996), Comprehensive Equation of State of Granular Materials, *Soils and Foundations*, 36, 1, 1–12.

Gudehus G., Nübel K. (2003), Evolution of Shear Bands in Sand, *Geotechnique* (in print).

Gutierrez M. A., de Borst R. (1998), Energy Dissipation, Internal Length Scale and Localization Patterning – a Probabilistic Approach, [in:] *Computational Mechanics* (S. Idelsohn, E. Onate, E. Dvorkin, eds,), CIMNE, Barcelona, 1–9.

Herle I., Gudehus G. (1999), Determination of Parameters of a Hypoplastic Constitutive Model from Properties of Grain Assemblies, *Mechanics of Cohesive-Frictional Materials*, 4, 5, 461–486.

Hobbs B. E., Ord A. (1989). Numerical Simulation of Shear Band Formation in Frictional-Dilational Materials, *Ingenieur-Archiv*, 59, 209–220.

Huang W., Nübel K., Bauer E. (2002). A Polar Extension of Hypoplastic Model for Granular Material with Shear Localization, *Mechanics of Materials*, 34, 563–576.

Kolymbas D. (1977), A Rate-Dependent Constitutive Equation for Soils, *Mechanics Research Communications*, 4, 367–372.

Leśniewska D. (2000), Analysis of Shear Pattern Formation in Soil, *Institute of Hydroengineering of the Polish Academy of Sciences,* Gdańsk, 1–204.

Löffelmann F. (1989), Theoretische und Experimentelle Untersuchungen zur Schüttgut-Wand-Wechselwirkung und zum Mischen und Entmischen von Granulaten, *Dissertation*, Karlsruhe University.

Maier T. (2002), Numerische Modellierung der Entfestigung im Rahmen der Hypoplastizität, *PhD Thesis,* Dortmund University, Germany.

Marcher T., Vermeer P. A. (2001), Macromodelling of Softening in Non-Cohesive Soils, [in:] *Continous and Discontinous Modelling of Cohesive-Frictional Materials*, eds. P. A. Vermeer et al, Springer-Verlag, 89–110.

Mühlhaus H. B. (1989), Application of Cosserat Theory in Numerical Solutions of Limit Load Problems, *Ing. Arch.*, 59, 124–137.

Mühlhaus H. B. (1990), Continuum Models for Layered and Blocky Rock, [in:] *Comprehensive Rock Engineering*, eds. J. A. Hudson, Ch. Fairhurst, Pergamon Press, 2, 209–231.

Nübel K., Karcher C. (1998), FE Simulations of Granular Material with a Given Frequency Distribution of Voids as Initial Condition, *Granular Matter*, 1, 3, 105–112.

Nübel K. (2002), Experimental and Numerical Investigation of Shear Localization in Granular Materials, *Publication Series of the Institute of Soil and Rock Mechanics*, University Karlsruhe, 140, 1–159.

Oda M., Konishi J., Nemat-Nasser S. (1982), Experimental Micromechanical Evaluation of Strength of Granular Materials, Effects of Particle Rolling, [in:] *Mechanics of Materials*, North-Holland Publishing Comp., 1, 269–283.

Oda M. (1993), Micro-Fabric and Couple Stress in Shear Bands of Granular Materials, [in:] *Powders and Grains*, ed. C. Thornton, Rotterdam, Balkema, 161–167.

Oda M., Tatsuoka F., Yoshida T. (1997), Void Ratio in Shear Band of Dense Granular Soils, [in:] *Deformation and Progressive Failure in Geomechanics*, eds. A. Asaoka, T. Adachi and F. Oka, Pergamon, 157–162.

Pamin J. (1994), Gradient-Dependent Plasticity in Numerical Simulation of Localisation Phenomena, *PhD Thesis*, Delft University, 1–134.

Schäfer H. (1962), Versuch einer Elastizitätstheorie des zweidimensionalen ebenen Cosserat-Kontinuums, *Miszellaneen der Angewandten Mechanik*, Festschrift Tolmien W., Berlin, Akademie-Verlag.

Shahinpoor M. (1981), Statistical Mechanical Considerations on Storing Bulk Solids, *Bulk Solid Handling*, 1, 1, 31–36.

Shi Q., Chang C. S. (2003), Numerical Analysis for the Effect of Heterogeneity on Shear Band Formation, *Proc. 16th ASCE Engineering Mechanics Conference,* University of Washington, Seattle, 1–11.

Sluys L. J. (1992), Wave Propagation, Localisation and Dispersion in Softening Solids, *PhD Thesis*, Delft University of Technology.

Steinmann P. (1995), Theory and Numerics of Ductile Micropolar Elastoplastic Damage, *Int. J. for Num. Meth. in Engng.*, 38, 583–606.

Tatsuoka F., Siddiquee M. S., Yoshida T., Park C. S., Kamegai Y., Goto S., Kohata Y. (1994), Testing Methods and Results of Element Tests and Testing Conditions of Plane Strain Model Bearing Capacity Tests using Air-Dried Dense Silver Buzzard Sand, *Internal Report*, University of Tokyo, 1–129.

Tatsuoka F., Goto S., Tanaka T., Tani K., Kimura Y. (1997), Particle Size Effects on Bearing Capacity of Footing on Granular Material, [in:] *Deformation and Progressive Failure in Geomechanics*, eds.: A. Asaoka, T. Adachi and F. Oka, Pergamon, 133–139.

Tejchman J. (1989), Scherzonenbildung und Verspannungseffekte in Granulaten unter Berücksichtigung von Korndrehungen, *Publication Series of the Institute of Soil and Rock Mechanics*, University Karlsruhe, 117, 1–236.

Tejchman J., Wu W. (1993), Numerical Study on Shear Band Patterning in a Cosserat Continuum, *Acta Mechanica*, 99, 61–74.

Tejchman J. (1997), Modelling of Shear Localisation and Autogeneous Dynamic Effects in Granular Bodies, *Publication Series of the Institute of Soil and Rock Mechanics*, University Karlsruhe, 140, 1–353.

Tejchman J., Wu W. (1997), Dynamic Patterning of Shear Bands in a Cosserat Continuum, *International Journal of Engineering Mechanics ASCE*, 123, 2, 123–134.

Tejchman J., Herle I., Wehr J. (1999), FE–Studies on the Influence of Initial Void Ratio, Pressure Level and Nean Grain Diameter on Shear Localisation, *Int. J. Num. Anal. Meth. Geomech.*, 23, 2045–2074.

Tejchman J., Gudehus G. (2001), Shearing of a Narrow Granular Strip with Polar Quantities, *J. Num. and Anal. Methods in Geomechanics*, 25, 1–18.

Tejchman J. (2002), Patterns of Shear Zones in Granular Materials within a Polar Hypoplastic Continuum, *Acta Mechanica*, 155, 1–2, 71–95.

Tejchman J. (2003a), FE-Studies on Formation of Shear Zones in Granular Bodies within a Polar Hypoplasticity, [in:] *Bifurcation and Instabilities in Geomechanics*, eds. J. F. Labuz and A. Drescher, Balkema, 133–149.

Tejchman J. (2003b), A Non-Local Hypoplastic Constitutive Law to Describe Shear Localizations in Granular Bodies, *Archives of Hydro-Engineering and Environmental Mechanics*, 50, 4, 229–250.

Tejchman J. (2004a), Comparative FE-Studies on Shear Localizations in Granular Bodies within a Polar and Non-Local Hypoplasticity, *Mechanics Research Communications*, 31, 341–354.

Tejchman J. (2004b), A Gradient Hypoplastic Constitutive Law to Describe Shear Localizations in Granular Bodies, *Archives of Hydro-Engineering and Environmental Mechanics* (submitted).

Tejchman J., Bauer E. (2004), Effect of Cyclic Shearing on Shear Localisation in Granular Bodies, *Granular Matter*, 5, 201–212.

Uesugi M., Kishida H., Tsubakihara Y. (1988), Behaviour of Sand Particles in Sand-Steel Friction, *Soils and Foundations*, 28, 1, 107–118.

Wang C. C. (1987), A New Representation Theorem for Isotropic Functions, *J. Rat. Mech. Anal.*, 36, 166–223.

von Wolffersdorff P. A. (1996), Hypoplastic Relation for Granular Materials with a Predefined Limit State Surface, *Mechanics Cohesive-Frictional Materials*, 1, 251–271.

Wu W. (1992), Hypoplasticity as a Mathematical Model for the Mechanical Behaviour of Granular Materials, *Publication Series of the Institute for Soil Mechanics*, Karlsruhe University, 129, 1–154.

Wu W., Niemunis A. (1996), Failure Criterion, Flow Rule and Dissipation Function Derived from Hypoplasticity, *Mechanics of Cohesive-Frictional Materials*, 1, 145–163.

Vardoulakis I. (1977), Scherfugenbildung in Sandkörpern als Verzweigungsproblem, *Dissertation*, Institute for Soil and Rock Mechanics, University of Karlsruhe.

Vardoulakis I. (1980), Shear Band Inclination and Shear Modulus in Biaxial Tests, *Int. J. Num. Anal. Meth. Geomech.*, 4, 103–119.

Yoshida Y., Tatsuoka T., Siddiquee M. (1994), Shear Banding in Sands Observed in Plane Strain Compression, [in:] *Localisation and Bifurcation Theory for Soils and Rocks*, eds.: R. Chambon, J. Desrues and I. Vardoulakis, Balkema, Rotterdam, 165–181.

Zervos A., Papanastasiou P., Vardoulakis I. (2001), A Finite Element Displacement Formulation for Gradient Elastoplasticity, [in:] *Bifurcation and Localisation Theory in Geomechanics* eds.: H. B. Mühlhaus, A. Dyskin and E. Pasternak, Balkema, 177–187.